Experimental and numerical analysis of short-pulse laser interaction with tissue phantoms containing inhomogeneities

Champak Das, Ashish Trivedi, Kunal Mitra, and Tuan Vo-Dinh

The objective is to perform an experimental and numerical study to analyze short-pulse laser propagation through tissue phantoms without and with inhomogeneities embedded in them. For a short-pulse laser the observed optical signal has a distinct temporal shape, and the shape is a function of the medium properties. The scattered temporal transmitted and reflected optical signals are measured experimentally with a streak camera for tissue phantoms irradiated with a short-pulse laser source. A parametric study involving different scattering and absorption coefficients of tissue phantoms and inhomogeneities, as well as the detector positions and orientations, is performed. The temporal and spatial profiles of the scattered optical signals are compared with the numerical modeling results obtained by solving the transient radiative transport equation by using the discrete ordinates technique. © 2003 Optical Society of America

OCIS codes: 140.0140, 170.0170, 170.3660, 170.6920.

1. Introduction

The study of short-pulse laser radiation transport through highly scattering media has received increasing attention during the past few years as a result of its wide applications such as optical imaging for medical diagnosis,[1–4] surgical and therapeutics,[5–8] remote sensing,[9,10] and material processing.[11] The nascent field of optical tomography for biomedical imaging that uses short-pulse lasers is made possible by a spectral window in the infrared wavelength region in which light absorption is small and scattering dominates.[3,12–14] Optical methods are a recent addition to the arsenal of noninvasive diagnostic tools available for the detection of disease, such as x-ray computed tomography, magnetic resonance imaging, positron emission tomography, single-photon-emission computed tomography, ultrasound imaging, and electrical impedance tomography.[15] The potential of optical tomography as a new diagnostic tool has stimulated considerable interest in the past ten years. Although limited to approximately the first 5 cm of the body, the technique offers several advantages often not available in established imaging modalities such as ultrasound, x-ray computed tomography, and magnetic resonance imaging. These benefits include nonionizing radiation, relatively inexpensive instrumentation, and the potential for functional (i.e., spectroscopic) imaging of optical tissue properties. In functional imaging, light at specific wavelengths can be used to excite specific biological molecules of interest, such as nicotinamide adenine dinucleotide (NAD or NADH), tryptophan, and hemoglobin, to provide real-time, *in vivo* information on the functional status of tissues and organs (e.g., pH, tissue oxygenation, glucose, dysplasia, tumor). Luminescence techniques based on bioluminescence allow the monitoring of gene expression *in vivo* in animals for drug discovery investigations. Two basic measurement methodologies are used for optical tomography: (1) frequency-domain methods that employ harmonically modulated photon density waves and phase-resolved detection, which measures the phase shift of the photon density waves,[16–19] and (2) time-resolved methods that use pulsed excitation and gated detection to examine the response of tissue to a short pulse of incident light. In this paper, the

C. Das, A. Trivedi, and K. Mitra (kmitra@fit.edu), the corresponding author (kmitra@fit.edu), are with Department of Mechanical and Aerospace Engineering, Florida Institute of Technology, 150 West University Boulevard, Melbourne, Florida 32901. T. Vo-Dinh (vodinht@ornl.gov) is with Oak Ridge National Laboratory, P.O. Box 2008, M.S. 6101, Oak Ridge, Tennessee 37831-6101.

Received 12 December 2002; revised manuscript received 20 May 2003.

0003-6935/03/255173-08$15.00/0

use of time-resolved techniques are investigated. In optical tomography a short-pulse laser is focused on the region to be probed and the time-dependent scattered reflected and transmitted signals are measured at different locations by using ultrafast detectors. It is the intent of the method to reconstruct the image of the interior and determine optical properties of the tissue medium from the time-resolved intensity measurements.

Short-pulse laser-probing techniques for diagnostics have distinct advantages over large pulse width or continuous-wave (cw) lasers primarily because of the additional information conveyed by the temporal distribution of the observed signal.[20,21] The distinct feature is the multiple-scattering-induced temporal distributions, which persist for a time period greater than the duration of the source pulse and are a function of the source pulse width as well as the optical properties of the medium. If the detection is carried out at the same short time scale (comparable with the order of the pulse width), the signal continues to be observed even at large times after the pulse has been off, owing to the time taken for the photons to migrate to the detector after multiple scattering in the media. Forward- and backward-radiative transport models for determination of optical properties of the tissue interior from transmitted and reflected signal measurements can therefore be based on the full temporal signal.[22–24] On the other hand, when conventional cw laser sources are utilized, the information available is the magnitude of the net attenuation and the angular distribution of the transmitted or reflected signal, which do not provide useful information about medium properties.

Other techniques that are commonly used for biomedical imaging focus on the initial transients of the temporal signal. Time gating,[25] optical coherence interferometry techniques,[26] and streak camera applications[27] have been used for evaluating the earliest arriving photons. However, these ballistic components may not be of practical use for tissues thicker than a few centimeters because they are not measurable with increasing tissue thickness. The frequency-domain techniques developed for biomedical imaging also suffer from low resolution because of to the nonavailability of a high-frequency source, restricting the temporal resolution to few nanoseconds.

To predict the optical properties of tissues from time-resolved scattered signal measurements, one must develop inverse algorithms. But before complex inverse algorithms can be developed, accurate forward solutions of the transient radiative transport equation (RTE) necessary to analyze short-pulse laser propagation through tissues are critical. In most previous analyses the transient term of the RTE is usually neglected. This assumption does not lead to errors, as the temporal variations of observed signals are slow compared with the time of flight of a photon. However, in applications involving short-pulse laser interactions with tissues, the transient effect must be considered in the RTE.[1,3,20,28,29]

The transient solution of the RTE for one-dimensional geometry for the case of short-pulse laser incidence has been developed and reported in the literature.[1,20,30–32] The research has been extended to two-dimensional geometry by using the simplified first-order spherical harmonics (P_1) approximation for a rectangular geometry.[33] Integral equation formulation techniques for the transient RTE have been also developed.[34,35] However, the P_1 model underestimates the speed of light propagation,[1,20] and the integral formulation is difficult to apply to complex geometries. The Monte Carlo method has been also used by many researchers.[36,37] The Monte Carlo method requires a large number of emitted bundles to obtain smooth accurate solutions, which is computationally expensive. The discrete ordinates method (DOM) has become popular for solving the transient RTE accurately and efficiently. The one-dimensional DOM has been used to analyze the transient radiant transfer in oceanographic lidar.[9] The DOM, in conjunction with the piecewise parabolic method scheme used previously to obtain numerical solutions for two-dimensional scattering–absorbing media, is used in this paper.[38]

No previous study has been reported in the literature that compares the experimentally measured scattered optical signals from a tissue phantom containing inhomogeneities due to short-pulse laser irradiation with accurate numerical solutions of the transient RTE. Such studies are critical for predicting the optical properties of tissues from temporal scattered optical signal measurements. In this paper the temporal optical transmitted and reflected signals from tissue phantoms without and with inhomogeneities embedded in them are measured with a streak camera. A parametric study involving different scattering and absorption coefficients of tissue phantoms and inhomogeneities, as well as the detector positions and orientations, is performed. The experimentally measured temporal scattered optical signals are compared with numerical modeling results obtained by solving the transient RTE by using the DOM.

2. Mathematical Formulation

In this paper the tissue base medium is approximated by an anisotropically scattering and absorbing rectangular enclosure in which an inhomogeneity is embedded (see Fig. 1). The transient RTE is given by[20,39]

$$\frac{1}{c}\frac{\partial I(x, y, \Omega, t)}{\partial t} + \mu\frac{\partial I(x, y, \Omega, t)}{\partial x} + \eta\frac{\partial I(x, y, \Omega, t)}{\partial y} + k_e I(x, y, \Omega, t) = \frac{k_s}{4\pi}\int_{4\pi} \Phi(\Omega', \Omega) I(x, y, \Omega', t)\mathrm{d}\Omega' + S(x, y, \Omega, t), \quad (1)$$

where I is the scattered diffuse intensity (watts per square meter per steradian), k_e and k_s are the extinction coefficient and the scattering coefficient, respectively, Φ is the phase function, Ω is the solid angle, c

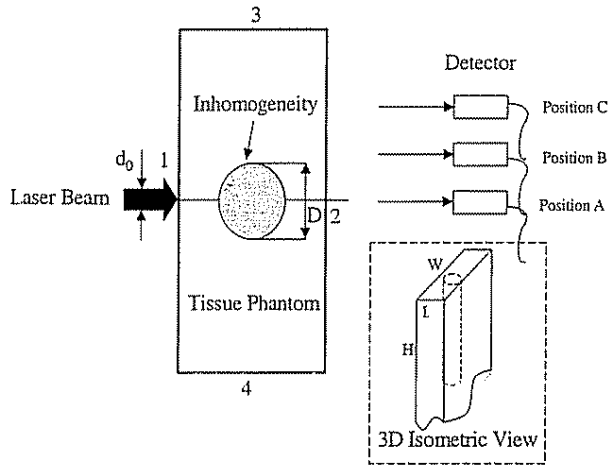

Fig. 1. Schematic of the problem under consideration.

is the velocity of light in the medium, x and y are the spatial coordinates, t is the time, and S is the source term.

The scattering phase function is represented by the Henyey–Greenstein function in terms of Legendre polynomials P_n as

$$\Phi(\Omega', \Omega) = \sum_{n=0}^{N} (2n + 1)\, g^n P_n[\cos(\Theta)], \qquad (2a)$$

where g is the asymmetry factor and N is the anisotropy factor. The higher the value of g and N, the more forward scattered is the phase function of the medium. Tissues usually are a highly forward-scattered medium. Typical values of g vary from 0.75 to 0.9,[14] and N varies from 12 to 20. The scattering angle Θ is represented by

$$\cos(\Theta) = \mu\mu' + \eta\eta' + \xi\xi', \qquad (2b)$$

where μ, η, and ξ are the direction cosines of the light-propagation direction Ω.

The pulsed radiation incident on the tissue medium at face 1 (see Fig. 1) is a Gaussian-shaped pulse having a temporal duration (pulse width) t_p at full width half-maximum (FWHM). The intensity can be separated into a collimated component, corresponding to the incident source, and a scattered intensity. If I_c is the collimated intensity, then I is the remaining intensity described by Eq. (1). The collimated component of the intensity for the square pulse is represented by

$$I_c(x, y, \Omega, t) = I_0 \exp(-k_e x)\,[H(t - x/c) - H(t - t_p - x/c)]\partial(\Omega - \Omega_0), \qquad (3)$$

where I_0 is the intensity leaving the wall toward the medium, $H(t)$ is the Heaviside step function, and $\partial(t)$ is the Dirac delta function. The Gaussian pulse is approximated as a square pulse for ease of numerical implementation.

The source function S formed from the collimated irradiation is then given by

$$S(x, y, \Omega, t) = \frac{k_s}{4\pi}\int_{4\pi} \Phi(\Omega', \Omega) I_c(x, y, \Omega', t)\, d\Omega'. \qquad (4)$$

The boundary conditions are such that intensity leaving the boundary surface is composed of the contribution of the outgoing emitted intensity and the reflection of incoming radiation in direction Ω. The refractive indexes of the base tissue phantom and inhomogeneities are chosen to be same; then the laser beam does not change direction after entering the inhomogeneity.

In the DOM, the RTE and the associated boundary condition are replaced by a set of equations for a finite number of M directions that cover 4π-sr solid angles. The integral terms of Eqs. (1) and (4) are reformulated with the aid of an angular quadrature of order M.

The discrete form of the time-dependent RTE in the direction Ω_m is then represented as

$$\frac{1}{c}\frac{\partial I_m(x, y, t)}{\partial t} + \mu_m \frac{\partial I_m(x, y, t)}{\partial x} + \eta_m \frac{\partial I_m(x, y, t)}{\partial y} = -k_e I_m(x, y, t) + \frac{k_s}{4\pi}\sum_{m'=1}^{M} w_{m'} \Phi_{m'm} I_{m'}(x, y, t) + S_m(x, y, t), \qquad (5)$$

where $m = -M, \ldots, -1, 1, \ldots, M$ and $\{\Omega_m, w_m\}$ defines a quadrature of M discrete directions Ω_m with which the weights w_m are associated.

In this study the piecewise parabolic advection scheme already developed by the authors to solve the two-dimensional geometry is used in Eq. (5).[30,38,40,41] The left-hand side of Eq. (5) is treated by the upwind monotonic interpolation methods. The piecewise parabolic advection scheme is efficient and produces a small amount of diffusion.

3. Tissue Phantoms

The tissue phantoms used in this study are made of Araldite 502 embedding medium. Araldite 502 resin is polymerized with dodecenyl succinic anhydride and catalyzed with 2, 4, 6-triphenol (DMP-30) in the volumetric ratio of 1:0.85:0.04. The samples are cured overnight at 35 ° C, the next day at 45 °C, and then again overnight at 60 °C. The refractive index of the resin is 1.54. Titanium dioxide (mean diameter = 0.3 μm) is added as scatterers to the resin base. Red-colored dye is used as an absorber as its absorbance is highest at 514-nm wavelength. The scattering and absorption coefficients are varied by varying the concentration of titanium dioxide and dye in resin matrix.[42] Typical tissue phantom dimensions as shown in Fig. 1 are 25 mm [width (W)] × 100 mm [height (H)] × 8 mm [thickness (L)]. Inhomogeneities typically of 4-mm diameter are drilled in the center of the samples and filled with different scat-

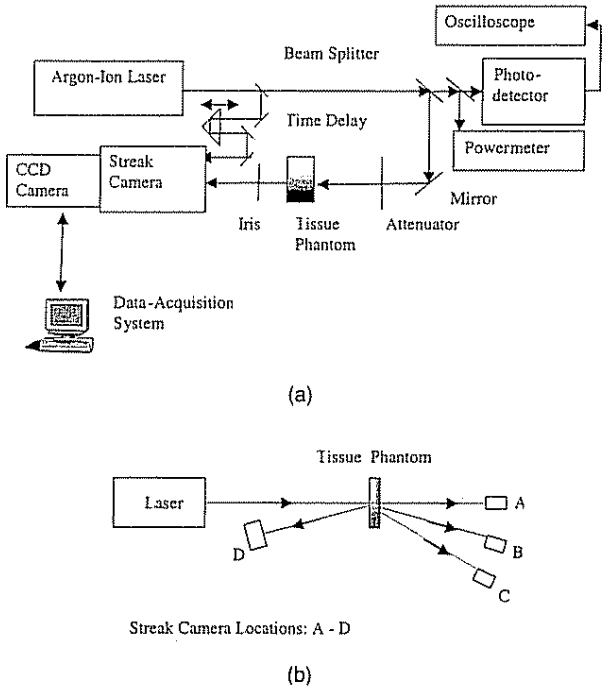

Fig. 2. (a) Schematic of the experimental setup. (b) Different measurement locations for transmittance (A–C) and reflectance (D).

tering coefficients other than the base resin matrix. This can be done either by recasting the tissue phantom filled with inhomogeneities or by casting the parts separately by using an index-matching liquid. Typical values for scattering and absorption coefficients used for tissue phantoms are 10 and 0.005 mm^{-1}, respectively. These values are consistent with tissue optical properties available in the literature.[14] The tissue phantoms are cast in aluminum molds. The tissue phantom has a strong adhesion property to aluminum as well as other metals. Silicon-based mold-release agents with crytox are sprayed on the molds before the phantom is cast, which facilitates easy removal of samples after they are cast.

4. Experimental Procedure

An argon–ion mode-locked laser having a pulse width (t_p) = 200 ps at FWHM operating at a frequency of 76 MHz and having a wavelength of 514 nm is used. Figure 2(a) shows the schematic of the experimental setup. The laser beam is split into two parts: one is used as the time reference, and the other is incident to the tissue phantom. A translation stage is introduced for an adjustable optical delay in the reference beam to be used as marker for the determination of the origin of the time scale. Attenuators are used to control incident power on tissue phantoms. The phantoms are placed in the translation stage for scanning in the spatial direction. The beam is incident on the phantom, and scattered transmitted and reflected signals are collected by use of a Hamamatsu streak camera unit. Figure 2(b) shows the different detector orientations for measurements. The streak unit comprises an ultrafast synchroscan unit with the frequency-tuning unit coupled with a Hamamatsu CCD camera. The time resolution of the streak camera used in this study is 10 ps. The streak camera's image-acquisition control is remotely done by using the HPDTA_32 software, which is also used for image processing. An image integration technique is used for collection of data, which helps to clearly distinguish noise from useful data for low-intensity transmitted optical signals. The streak camera is triggered from the mode locker at the rate of 76 MHz. The power and pulse width of the laser is monitored throughout the experiment by using a powermeter and ultrafast photodiode, respectively.

5. Results

Experimental investigations of the nature of interactions of a short-pulsed laser with tissue phantoms with and without inhomogeneities embedded in them are conducted. The experimental observations are validated with numerical modeling results obtained by solving a two-dimensional transient RTE by using the DOM. The sample height is large compared with the beam diameter, and hence a two-dimensional transient radiative transfer model is applied. Experiments are conducted on tissue phantoms to measure transmitted and reflected optical signals along the axis of the laser beam as well as at different angles. For numerical simulations, values of $g = 0.8$ and $N = 16$ are used. The computational time is approximately 2000 s on an Alpha workstation with a 633-MHz, 21164 CPU for 80 discrete ordinate quadratures, a spatial grid size of 0.5 mm, and a temporal grid size of 0.5 ps. The accuracy of the numerical results is validated by ensuring the results are independent of the grid sizes.

Figure 3(a) shows the normalized transmitted signal measurements obtained with a homogenous tissue phantom having a thickness (L) = 8 mm. The tissue phantom that has a scattering coefficient (k_s) = 10 mm^{-1} and an absorption coefficient (k_a) = 0.005 mm^{-1} is used. It is also observed that the experimental results agree with the numerical simulation results. It is also observed that the experimental results and numerical simulation differ by 5 ps, which is within the uncertainty of the streak camera. The repeatability of measured optical signals is within 1.5% as shown with uncertainty bars in Fig. 3(a). The time for the earliest arriving photon for the 8-mm phantom of refractive index (n) = 1.54 is 41.07 ps. The transmission signal values are zero until the photons traverse the phantom thickness. These values are consistent with both the numerical and the experimental measurements as observed in Fig. 3(a). Many previously used approximate models fail to capture this effect and provide unrealistic results for the transmitted signals even before light has traversed through the medium. Figure 3(b) shows the corresponding normalized scattered optical signals for an 8-mm-thick sample for different detector orientations corresponding to Fig. 2(b).

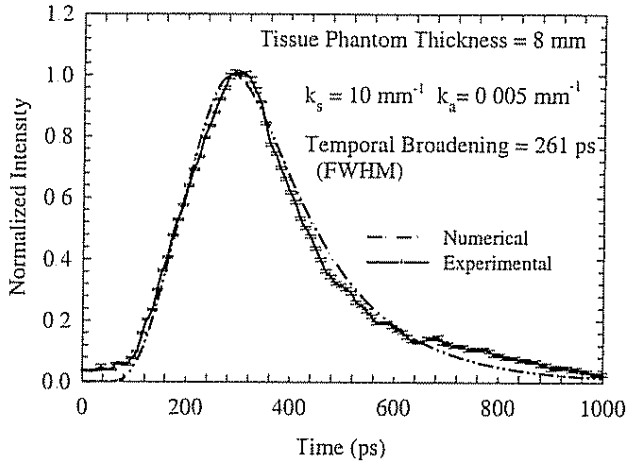

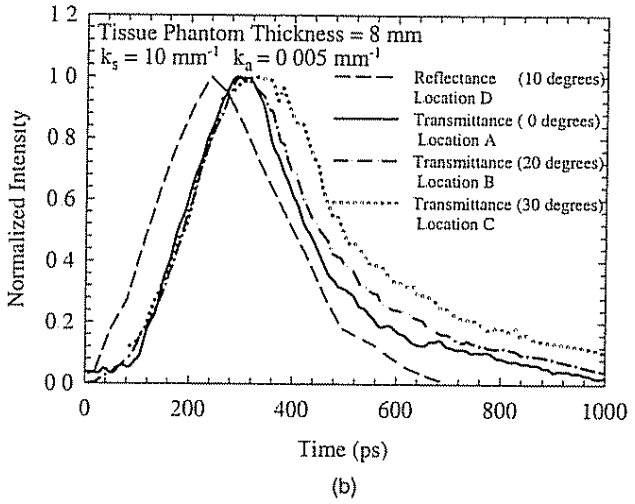

Fig 3 (a) Comparison of a temporal transmitted signal for a homogenous tissue phantom (b) Experimental measurements of temporal scattered signals for a homogenous tissue phantom at different detector angles

The photons measured in the forward direction have higher temporal broadening because of more multiple scattering.

Experiments are also conducted by varying the number of scatterers and therefore the scattering coefficient for the case of 8-mm-thick homogeneous tissue phantoms The experimentally measured normalized temporal transmitted signal profiles are plotted for various scattering coefficients (k_s = 5, 10, 15, and 20 mm^{-1}), keeping the absorption coefficient (k_a = 0.005 mm^{-1}) fixed. It is observed in Fig. 4 that the temporal spread increases with the increase of concentration of scatterers in the phantoms and hence the scattering coefficients as the phantoms undergo more multiple scattering. The magnitude of the signal also increases with the increase of the scattering coefficients but is masked owing to the normalization with respect to corresponding peak intensity values. The effect of the variation of the absorption coefficient (k_a = 0.005, 0.05, and 0.1 mm^{-1})

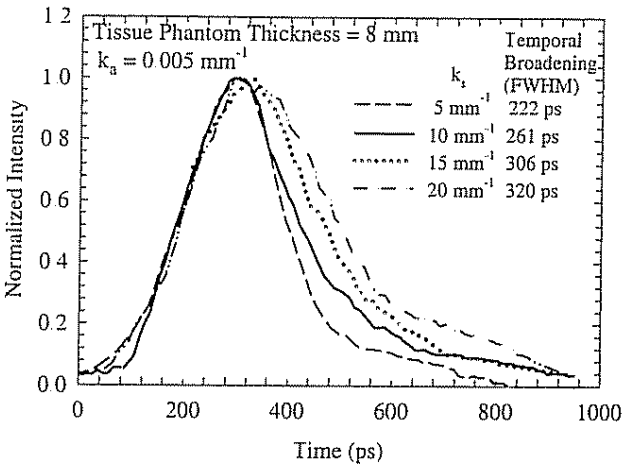

Fig 4 Effect of the scattering coefficient on the experimentally measured temporal transmitted signal for a homogeneous tissue phantom

of the tissue phantom on the experimentally measured transmitted optical signal is depicted in Fig. 5. The higher the absorption, the higher will be the attenuation of the laser beam and hence the lower the temporal broadening.

Figure 6 shows experimentally measured temporal profiles of a normalized transmitted signal for a tissue phantom containing an inhomogeneity measured at location A (see Fig. 1). Two cases are considered: one in which the inhomogeneity has higher scatterers (k_s = 20 mm^{-1}) compared with the tissue phantom (k_s = 10 mm^{-1}) and the other case in which the optical properties of the tissue phantom and the inhomogeneity are reversed. There is a reasonable match between numerical and experimental values with a little separation in the tail section. Figures 7(a) and 7(b) show corresponding spatial intensity profiles along the opposite face of incident radiation (face 2) for different times. The objective of these plots is to show the time instants at which the demarcation

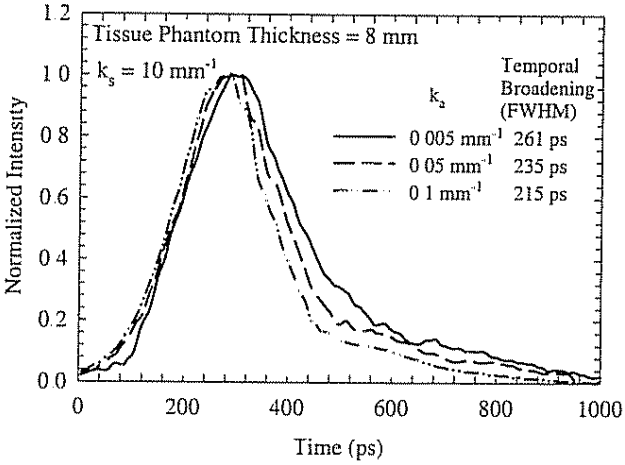

Fig 5 Effect of the absorption coefficient on the experimentally measured temporal transmitted signal for a homogeneous tissue phantom

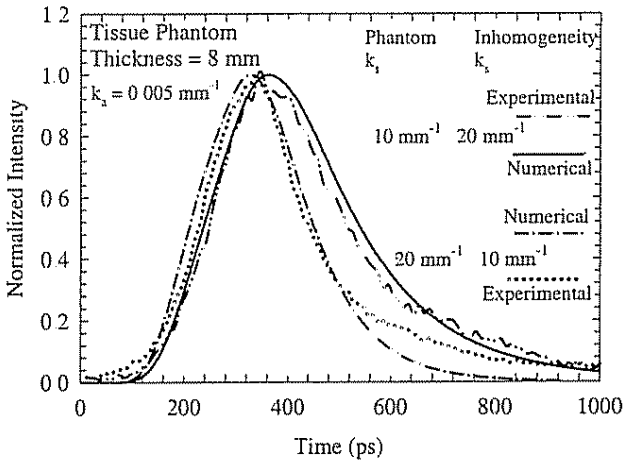

Fig 6 Comparison of a transmitted signal through a tissue phantom containing an inhomogeneity

between the tissue phantom and the inhomogeneity is most prominent. For both cases, detection of the inhomogeneity is difficult at small and large times. Within the time instant of 200 to 500 ps, demarcation between healthy tissue and the inhomogeneity is most prominent. It is interesting to observe in Figs. 7(a) and 7(b) that the spatial intensity profiles in the inhomogeneity region are reversed because the scattering coefficients of the tissue phantom and the inhomogeneity are reversed. On the other hand, it is not evident from the temporal transmitted signal presented in Fig. 6. The time instants at which demarcation between normal tissue and the inhomogeneity are most pronounced are also different because the light pulse travels initially through an optically less dense medium (lower scattering coefficient of the tissue phantom) in Fig. 7(a), and conditions are reversed in Fig. 7(b). It is observed that optical signals measured near the edges showed fluctuations due to boundary effects and hence are not shown in the figures.

Figure 8 shows the comparison between the numerical model and the experimental measurements for a particular time instant as presented in Figs. 7(a) and 7(b). The time instants selected correspond to the best contrast between the tissue phantom and the inhomogeneity. There is a reasonable match between experimental and numerical values. The spatial distribution of intensity along the face opposite to the incident face (2) is presented in Fig. 9 at a particular time instant for different scattering coefficients of the tissue phantom, keeping the inhomogeneity's optical properties constant. The normalized intensity is plotted in log scale to represent the high variation in the transmitted optical signal due to the difference in scattering coefficients between the tissue phantom and the inhomogeneity. This can be attributed to the fact that for one case the difference in scattering coefficients between the tissue phantom and the inhomogeneity is 4 times, whereas, in the other case, it is approximately 1.3 times. Therefore this results in a difference in magnitude of approximately 100 times in transmitted optical signals for these two cases.

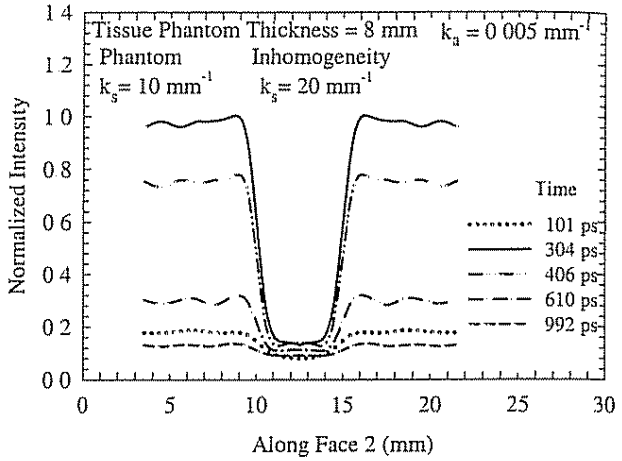

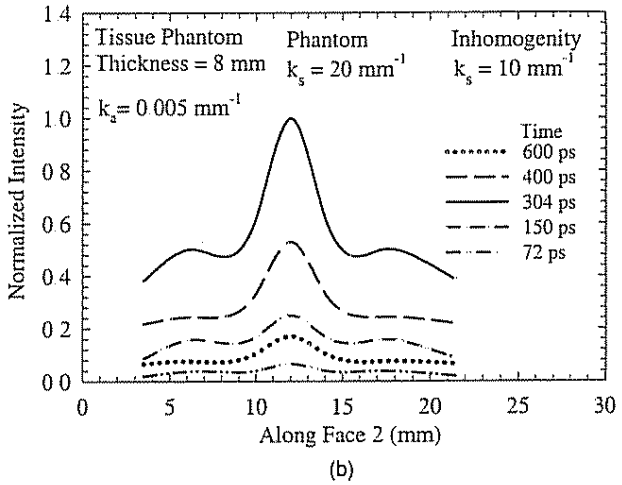

Fig 7 (a) Experimentally measured spatial intensity distribution for the case of the inhomogeneity that has a higher scattering coefficient than the tissue phantom has. (b) Experimentally measured spatial intensity distribution for the case of the inhomogeneity that has a lower scattering coefficient than the tissue phantom has.

The effect of the detector position on the transmitted signal obtained numerically is presented in Fig. 10. From Fig. 1 it is evident that the center of the inhomogeneity is on the same axis as the detector center. Therefore the detector position at the center receives more early arriving photons than the detectors farther away from the center. The temporal profiles for the detection positions at 6 and 9 mm from the center are appreciably shifted in the time axis compared with the one at the center. This is primarily because of the longer distance the photons need to travel in the tissue phantom before being detected by the streak camera. The temporal profile for the homogenous tissue phantom is also shown in the figure to demonstrate the temporal shift of the peak optical signal in the time axis as well as the earliest arriving time for the photons. These shifts

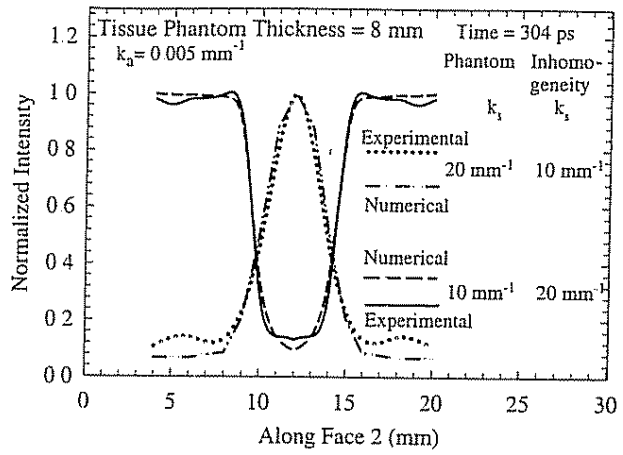

Fig. 8 Comparison of intensity profiles at a particular time for a tissue phantom containing an inhomogeneity.

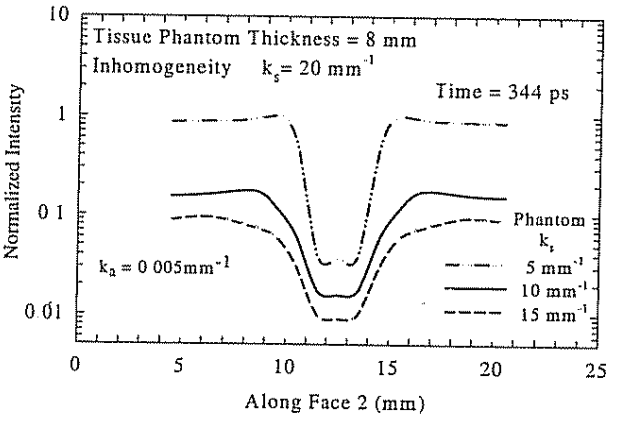

Fig. 9 Experimentally measured spatial intensity distribution for various scattering coefficients of the tissue phantom, keeping the inhomogeneity's optical properties constant.

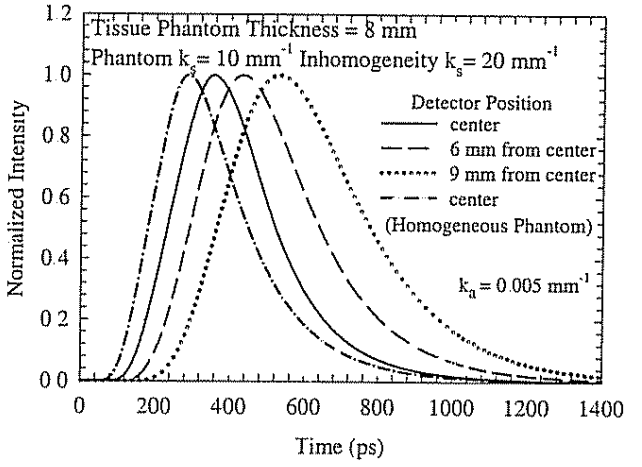

Fig. 10 Numerical simulation of temporal transmitted signals at different detector positions for a tissue phantom containing an inhomogeneity.

can definitely be predicted if any inhomogeneity is embedded inside a tissue phantom.

6. Conclusions

A comprehensive experimental and numerical investigation is performed to analyze short-pulse laser propagation through tissue medium that has embedded inhomogeneities. A parametric study, as performed in this paper, is critical to differentiate between a healthy tissue phantom and that containing an inhomogeneity. The transient discrete ordinates method, as used in this paper, is an accurate model to analyze the propagation of a short-pulse laser through scattering absorbing media such as tissues. Accurate validation of the forward transient radiative transport equation with the experimentally measured data is critical before inverse algorithms can be developed. Short-pulse laser probing for detection of tumors in tissues is a novel and nascent technology, and this research can be furthered by experiments on animal models.

Kunal Mitra acknowledges partial support from the Oak Ridge National Laboratory through contract 4000004751. Tuan Vo-Dinh acknowledges support from National Institutes of Health grant 1 R01 CA88787-01 and U.S. Department of Energy, Office of Environmental and Biological Research, under contract DE-AC05-00OR22725 with UT-Battelle, LLC.

References

1. S. Kumar and K. Mitra, "Microscale aspects of thermal radiation transport and laser applications," Adv. Heat Transfer **33**, 187–294 (1999).
2. S. A. Prahl, M. J. C. van Gemert, and A. J. Welch, "Determining the optical properties of turbid media by using the adding–doubling method," Appl. Opt. **32**, 559–568 (1993).
3. Y. Yamada, "Light–tissue interaction and optical imaging in biomedicine," Annu. Rev. Fluid Mech. Heat Transfer **6**, 1–59 (1995).
4. J. C. Hebden, H. Veenstra, H. Dehghani, E. M. C. Hillman, M. Schweiger, S. R. Arridge, and D. T. Delpy, "Three-dimensional time-resolved optical tomography of a conical breast phantom," Appl. Opt. **40**, 3278–3287 (2001).
5. G. J. R. Spooner, T. Juhasz, R. Imola, G. Djotyan, C. Horvath, Z. Sacks, G. Marre, D. Miller, A. R. Williams, and R. Kurtz, "New developments in ophthalmic applications of ultrafast lasers source," in *Commercial and Biomedical Applications of Ultrafast Lasers II*, J. Neev and M. K. Reed, eds., Proc. SPIE **3934**, 62–72 (2000).
6. J. E. Marion and B. M. Kim, "Medical applications of ultrashort-pulse lasers," in *Commercial and Biomedical Applications of Ultrafast Lasers*, M. K. Reed and J. Neev, eds., Proc. SPIE **3616**, 42–50 (1999).
7. R. M. Kurtz, V. Elner, X. Liu, T. Juhasz, F. H. Loesel, C. Horvath, M. H. Niemz, and F. Noack, "Plasma-mediated ablation of biological tissue with picosecond and femtosecond laser pulses," in *Laser–Tissue Interaction VIII*, S. L. Jacques, ed., Proc. SPIE **2975**, 192–200 (1997).
8. F. H. Loesel, A. C. Tien, S. Backus, H. Kapteyn, R. M. Murane, S. Sayegh, and T. Juhasz, "Effect of reduction of laser pulse width from 100 ps to 20 fs on the plasma-mediated ablation of hard and soft tissue," in *Thermal Therapy, Laser Welding, and Tissue Interaction*, S. G. Bown, G. P. Delacretaz, G. Godlewski,

G. J. Mueller, R. Pini, H. Reidenbach, R. W. Steiner, L. O. Svassand, and K. Tranberg, eds., Proc. SPIE **3565,** 116–123 (1999).
9. K. Mitra and J. H. Churnside, "Transient radiative transfer equation applied to oceanographic lidar," Appl. Opt. **38,** 889–895 (1999).
10. R. E. Walker and J. W. McLean, "Lidar equations for turbid media with pulse stretching," Appl. Opt. **38,** 2384–2397 (1999).
11. M. Gower, "Excimer laser microfabrication and micromachining," in *First International Symposium on Laser Precision Microfabrication,* I. Miyamoto, K. Sugioka, and T. W. Sigmon, eds., Proc. SPIE **4088,** 124–131 (2000).
12. A. Yodh and B. Chance, "Spectroscopy and imaging with diffusing light," Phys. Today **48,** 34–40 (1995).
13. E. C. Hillman, J. C. Bebden, M. Schweiger, H. Dehghani, F. W. Schmidt, D. T. Delpy, and S. R. Arridge, "Timer resolved optical tomography of the human forearm," Phys. Med. Biol. **46,** 1117–1130 (2001).
14. O. Jarlman, R. Berg, S. Andersson-Engels, S. Svanberg, and H. Pettersson, "Time-resolved white light transillumination for optical imaging," Acta Radiol. **38,** 185–189 (1997).
15. T. Vo-Dinh, ed., *Biomedical Photonics Handbook* (CRC Press, Boca Raton, Fla., 2003).
16. D. A. Boas, and A. G. Yodh, "Spatially varying dynamical properties of turbid media probed with diffusing temporal light correlation," J. Opt. Soc. Am. A **14,** 192–215 (1997).
17. B. J. Tromberg, L. O. Svaasand, T. Tsay, and R. C. Haskell, "Properties of photon density waves in multiple-scattering media," Appl. Opt. **32,** 607–617 (1993).
18. E. M. Sevick-Muraca, G. Lopez, T. L. Troy, J. S. Reynolds, and C. L. Hutchinson, "Fluorescence and absorption contrast mechanisms for biomedical optical imaging using frequency-domain techniques," Photochem. Photobiol. **66,** 55–64 (1997).
19. S. J. Norton and T. Vo-Dinh, "Diffraction tomographic imaging with photon density waves: an explicit solution," J. Opt. Soc. Am. A **15,** 2670–2677 (1998).
20. K. Mitra and S. Kumar, "Development and comparison of models for light-pulse transport through scattering–absorbing media," Appl. Opt. **38,** 188–196 (1999).
21. D. J. Hall, J. C. Hebden, and D. T. Deply, "Imaging very-low-contrast objects in breastlike scattering media with a time-resolved method," Appl. Opt. **36,** 7270–7276 (1997).
22. A. H. Hielscher, A. Klose, D. Catarious, and K. M. Hanson, "Tomographic imaging of biological tissue by time resolved, model based, iterative image reconstruction," in *Advances in Optical Imaging and Photon Migration,* J. G. Fujimoto and M. S. Patterson, eds. Vol. 21 of OSA Trends in Optics and Photonics Series (Optical Society of America, Washington, D.C., 1998), pp. 125–127.
23. S. R. Arridge, "The forward and inverse problem in time resolved infrared imaging," in *Medical Optical Tomography: Functional Imaging and Monitoring,* G. Muller, ed. (SPIE Press, Bellingham, 1993).
24. J. R. Singer, F. A. Grunbaum, P. Kohn, and J. P. Zubelli, "Image reconstruction of the interior of bodies that diffuse radiation," Science **248,** 990–991 (1990).
25. L. Wang, P. P. Ho, C. Liu, G. Zhang, and R. R. Alfano, "Ballistic 2-D imaging through scattering walls using an ultrafast Kerr gate," Science **253,** 769–771 (1991).
26. D. Huang, E. A. Swanson, C. P. Lin, J. S. Schuman, W. G. Stinson, W. Chang, M. R. Hee, T. Flotte, K. Gregory, C. A. Puliafito, and J. G. Fujimoto, "Optical coherence tomography," Science **254,** 1178–1181 (1991).
27. J. C. Hebden, "Evaluating the spatial resolution performance of time-resolved optical imaging system," Med. Phys. **19,** 1081–1087 (1992).
28. M. Q. Brewester and Y. Yamada, "Optical properties of thick turbid media from picosecond time-resolved light scattering measurement," Int. J. Heat Mass Transfer **8,** 2569–2581 (1995).
29. A. Ishimaru, "Diffusion of light in turbid material," Appl. Opt. **28,** 2210–2215 (1989).
30. M. Sakami, K. Mitra, and T. Vo-Dinh, "Analysis of short-pulse laser photon transport through tissues for optical tomography," Opt. Lett. **27,** 336–338 (2002).
31. M. Sakami, K. Mitra, and P. Hsu, "Transient radiative transfer in anisotropically scattering media using monotonicity-preserving schemes," International Mechanical Engineering Congress and Exposition **366-1,** 135–143 (2000).
32. S. Kumar, K. Mitra, and Y. Yamada, "Hyperbolic damped-wave models for transient light-pulse propagation in scattering media," Appl. Opt. **35,** 3372–3378 (1996).
33. K. Mitra, M. S. Lai, and S. Kumar, "Transient radiation transport in participating media within a rectangular enclosure," J. Thermophys. Heat Transfer **11,** 409–414 (1997).
34. Z. M. Tan and P. F. Hsu, "An integral formulation of transient radiative transfer," ASME J. Heat Transfer **123,** 466–475 (2001).
35. C. Y. Wu and S. H. Wu, "Integral equation formulation for transient radiative transfer in an anisotropically scattering medium," Int. J. Heat Mass Transfer **43,** 2009–2020 (2000).
36. A. H. Gandbakche, R. Nossal, and R. F. Bonner, "Scaling relationships for theories of anisotropic random walks applied to tissue optics," Appl. Opt. **32,** 504–516 (1993).
37. A. Sawetprawichkul, P. F. Hsu, K. Mitra, and M. Sakami, "A Monte Carlo study of the transient radiative transfer within the one-dimensional multi-layered slab," International Mechanical Engineering Congress and Symposium, Orlando (Florida) **366-1,** 145–153 (2000).
38. M. Sakami, K. Mitra, and P. F. Hsu, "Analysis of light-pulse transport through two-dimensional scattering-absorbing media," J. Quant. Spectrosc. Radiat. Transfer **73,** 169–179 (2002).
39. M. F. Modest, *Radiative Heat Transfer* (McGraw-Hill, New York, 2003).
40. G. Strang, "On the construction and comparison of difference schemes," SIAM J. Numer. Anal. **5,** 506–517 (1968).
41. P. Colella and P. R. Woodward, "The piecewise parabolic method for gas-dynamical simulations," J. Comput. Phys. **54,** 174–201 (1984).
42. M. Firbank and D. T. Delpy, "A design for a stable and reproducible phantom for use in near infra-red imaging and spectroscopy," Phys. Med. Biol. **38,** 847–853 (1993).